



ELSEVIER

Contents lists available at ScienceDirect

## Journal of Magnetism and Magnetic Materials

journal homepage: [www.elsevier.com/locate/jmmm](http://www.elsevier.com/locate/jmmm)

## Magnetic properties of nanoparticles of cobalt chromite

Chandana Rath<sup>a,\*</sup>, P. Mohanty<sup>a</sup>, A. Banerjee<sup>b</sup><sup>a</sup> School of Materials Science & Technology, Institute of Technology, Banaras Hindu University, 221 005 Varanasi, India<sup>b</sup> UGC-DAE Consortium for Scientific Research, Khandwa Road, 452017 Indore, India

## ARTICLE INFO

## Article history:

Received 10 July 2010

Received in revised form

25 January 2011

Available online 3 February 2011

## Keywords:

Nanoparticle

Chromite

Spinel

Superparamagnetism

Exchange bias

## ABSTRACT

Magnetic properties of cobalt chromite nanoparticles of size 8–12 nm synthesized through conventional coprecipitation route are reported. Magnetization versus temperature measurement plot reveals a transition from paramagnetic to superparamagnetic (SPM) phase in contrast with the transition from paramagnetic to long-range ferrimagnetic phase at Curie temperature,  $T_c$ , reported in bulk. The blocking temperature,  $T_b$ , of SPM phase is found to be 50–60 K. On cooling in the presence of 10 kOe field these nanoparticles show an enhancement in coercivity and shifting of loop at 10 K, which is absent at 50 K. While the later observation supports the blocking temperature of the SPM phase, the former one is attributed to a disordered spin configuration at the surfaces and the distribution of nanoparticle sizes.

© 2011 Elsevier B.V. All rights reserved.

## 1. Introduction

Chromite, cubic normal spinel compounds have recently attracted much attention as multiferroic materials [1]. Cobalt chromite ( $\text{CoCr}_2\text{O}_4$ ), one of the spinel family, is ferrimagnetic in nature in which magnetic  $\text{Co}^{2+}$  ions occupy A site and magnetic  $\text{Cr}^{3+}$  ions occupy B site [2]. The strong interactions among chromium ions in chromite control the magnetic order [3–5]. The antiferromagnetic alignment between A and B sites is completely destroyed and system exhibits a screw ordering. This is otherwise named as ferrimagnetic spiral wherein the spins lie on the conical surfaces. The magnetic order is mostly studied in bulk and single crystals. Menyuk et al. [6] studied the magnetic ordering through neutron diffraction and magnetic measurements of bulk samples and have shown that below  $T_c$ , magnetic ordering consists of a ferrimagnetic component and a spiral component. The ferrimagnetic component exhibits long range order at all temperatures below  $T_c$  while the spiral component exhibits a short range order. Tomiyasu et al. [7] revisited the spiral ordering by neutron scattering and magnetic measurements in  $\text{CoCr}_2\text{O}_4$  single crystals and report a simultaneous formation of long range order of ferrimagnetic component and a short range order of the spiral component at lowest temperature phase. In addition to the magnetic order investigated by Menyuk et al. [6] in polycrystalline sample, a dielectric anomaly below spiral magnetic order has been observed in polycrystalline sample [8] as well as in single crystals [1,9]. The spiral component

induces the electric polarization and also a spontaneous magnetization for which it is said to be as multiferroic. Due to lack of studies on nanoparticles of cobalt chromite, we have synthesized these particles in nanometer range by conventional coprecipitation route and studied the magnetic properties of these materials by varying temperature and magnetic field. We observed a transition from paramagnetic to superparamagnetic (SPM) phase at  $T_c$  instead of a transition from paramagnetic to ferrimagnetic phase. These nanoparticles exhibit an exchange bias phenomena below  $T_b$ .

## 2. Experimental methods

## 2.1. Synthesis of cobalt chromite powder

Conventional coprecipitation technique was used to synthesize cobalt chromite powders. We have used cobalt nitrate hexahydrate,  $\text{Co}(\text{NO}_3)_2 \cdot 6\text{H}_2\text{O}$  (molecular weight 291.03 g, 99%), chromium nitrate nonahydrate,  $\text{Cr}(\text{NO}_3)_3 \cdot 9\text{H}_2\text{O}$  (molecular weight 400.15 g, 98%) and ammonia solution (30% by weight) to synthesize cobalt chromite. Acetone of analytical grade was used for drying the precipitate. Stock solutions of cobalt nitrate (0.5 M), chromium nitrate (0.5 M) and ammonia solution (1.5 M) were prepared in 500 ml volumetric flasks separately by dissolving appropriate amount of  $\text{Co}(\text{NO}_3)_2 \cdot 6\text{H}_2\text{O}$ ,  $\text{Cr}(\text{NO}_3)_3 \cdot 9\text{H}_2\text{O}$  and  $\text{NH}_3$  (about 30%) in double distilled water respectively. From the stock solution, desired quantity of cobalt nitrate was taken in a 1000 ml beaker. Desired quantity of chromium nitrate solution was added slowly to the cobalt nitrate solution under continuous stirring. The mixed solution was further stirred at room temperature

\* Corresponding author.

E-mail address: [chandana.rath@yahoo.com](mailto:chandana.rath@yahoo.com) (C. Rath).

for 2 h. Further, aqueous ammonia solution (1.5 M) was added dropwise to the mixed solution till the pH of 8.9 was attained. The hydroxide precipitate was filtered, washed several times with distilled water till the filtrate attains a pH value of about 7. Finally the hydroxide precipitate was washed with acetone and was dried in an oven at 120 °C for 16 h to get the desired oxide. The dried oxide was calcined at 600 °C for 4 h to get well crystalline phase.

## 2.2. Characterization of cobalt chromite powder

The calcined powders were characterized by X-ray Diffraction (XRD) using an 18 kW rotating anode (Cu K<sub>α</sub>) based Rigaku powder

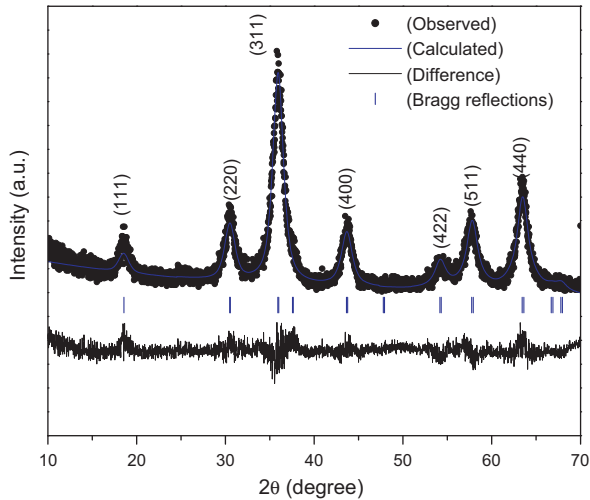


**Fig. 1.** X-ray diffraction spectrum of calcined CoCr<sub>2</sub>O<sub>4</sub> nanoparticles synthesized at pH 8.9 and fitted using Fullprof program with Fd3m space group. The observed pattern, calculated data after Le-Bail analysis and the difference pattern between observed and calculated one are shown as dots, continuous line and as bottom line, respectively.

Diffraction operating in the Bragg–Brentano geometry and fitted with a graphite monochromator in the diffracted beam. Field emission scanning electron microscopy (FESEM, ZEISS: SUPRA 40) at 5 kV is used for structural characterization of CoCr<sub>2</sub>O<sub>4</sub> nanoparticles. We measured the temperature and field dependent dc magnetization using Vibrating Sample Magnetometer insert of Physical Properties Measurement System (PPMS-VSM) of Quantum Design operating between 2 to 350 K. For frequency dependent ac susceptibility measurements SQUID magnetometer (Quantum Design) is used. We measured specific heat as a function of temperature using the heat capacity insert of PPMS (Quantum Design) for 8 mg pressed powder rectangular bar.

## 3. Results and discussion

**Fig. 1** depicts the XRD pattern of CoCr<sub>2</sub>O<sub>4</sub> calcined at 600 °C. The pattern is fitted using Fullprof program with Fd3m space group. The observed pattern, calculated data after Le-Bail analysis and the difference pattern between observed and calculated one are shown as dots, continuous line and as bottom line, respectively. The tick marks above the difference plot show the positions of the Bragg peaks. The well defined peaks corresponding to miller indices (1 1 1), (2 2 0), (3 1 1), (4 0 0), (4 2 2), (5 1 1) and (4 4 0) are ascribed to cubic phase of CoCr<sub>2</sub>O<sub>4</sub> (JCPDS file no:780711). No peaks other than CoCr<sub>2</sub>O<sub>4</sub> have been observed. The lattice parameter is found to be 8.310 Å, which is in agreement with the bulk value (8.334 Å). The mean crystallite diameter along (3 1 1) calculated using the Scherrer formula after correcting the instrumental broadening is found to be ~8 nm. Field emission scanning electron micrograph is shown in **Fig. 2**. The particles are mostly agglomerated and majority of particles are in 8–12 nm range as observed from particle size distribution histogram shown as inset of **Fig. 2**. Crystallite size is in good agreement with the particle size measured from FESEM.

**Fig. 3a** shows magnetization as a function of temperature under zero field cooling (ZFC) and field cooling (FC) condition

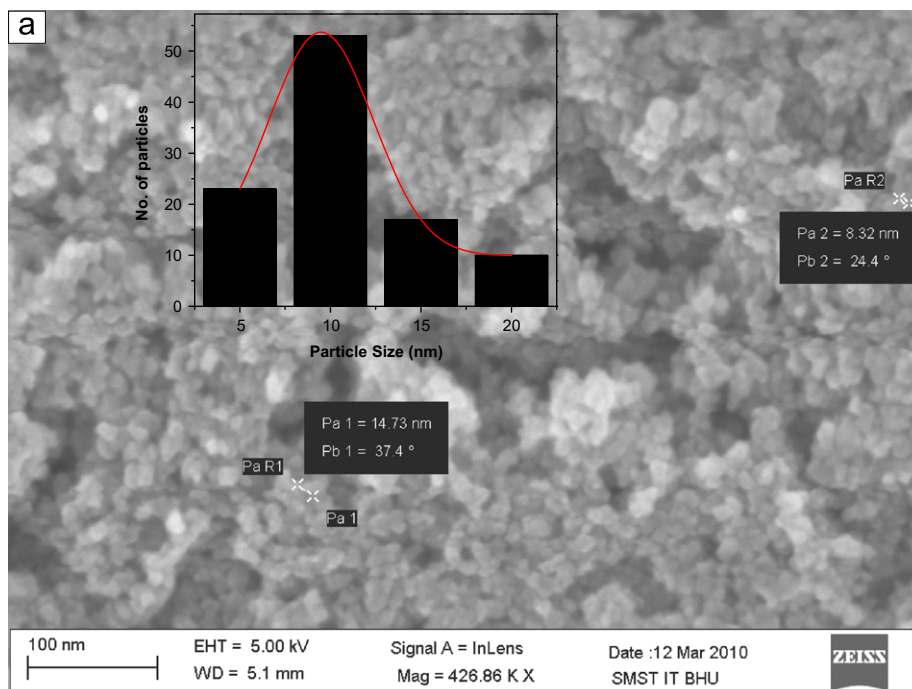


**Fig. 2.** Field Emission Scanning Electron Micrograph of CoCr<sub>2</sub>O<sub>4</sub> nanoparticles calcined at 600 °C and inset shows the particle size distribution histogram.

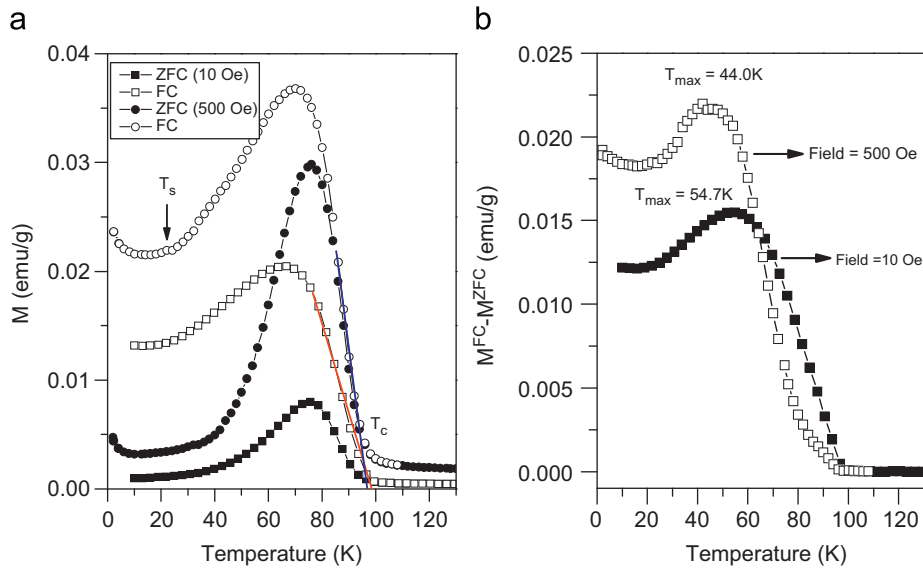


**Fig. 3.** (a) Temperature dependent zero field cooled (ZFC) and field cooled (FC) dc magnetization measured at  $H=500$  and  $10$  Oe. (b) Difference in magnetization observed after field cooling and zero field cooling at  $10$  and  $500$  Oe plotted with respect to change in temperature.

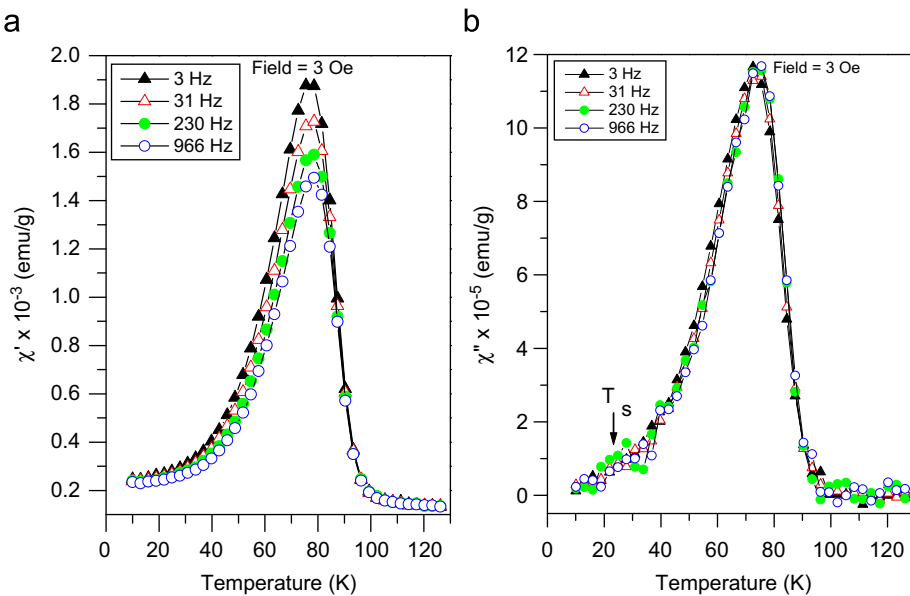


**Fig. 4.** (a) Real and (b) imaginary parts of ac susceptibility versus temperature measured at  $3$  Oe field and at different frequencies such as  $3$ ,  $31$ ,  $230$  and  $966$  Hz.

with field  $500$  and  $10$  Oe, respectively. ZFC does not fall upon FC curve. The branching in FC and ZFC starts at  $96$  and  $99$  K, respectively, in applied field of  $500$  and  $10$  Oe.  $T_c$  is derived by extrapolating the linear part of magnetization to zero in high temperature regime. It is found to be  $97$  K and  $98.5$  K which matches well with the  $T_c$  of bulk [1] and single crystals [7] of  $\text{CoCr}_2\text{O}_4$ . This suggests that  $T_c$  remains unaffected by reducing the size to nanoscale range. However, in similar kind of spinel structures like in ferrites, a large increase in  $T_c$  has been reported by reducing the size to nanoscale range [10,11]. Below  $T_c$ , magnetization shows a large increase in both ZFC and FC curves and then decreases further with decrease in temperature. An anomaly around a temperature  $\sim 23$  K in FC is observed in  $M$  versus  $T$  curve obtained by applying field of  $500$  Oe. This temperature is known as spiral ordering temperature,  $T_s$ . In bulk and single crystals of  $\text{CoCr}_2\text{O}_4$ ,  $T_s$  is observed at  $31$  and  $24$  K, respectively [7,8].  $T_s$  in our case lies in between  $T_s$  of bulk and single

crystals. Comparing the  $M^{\text{ZFC}}$  and  $M^{\text{FC}}$  values with bulk and single crystals, we observe no negative magnetization in  $M^{\text{ZFC}}$  as found in bulk samples [8] and an order of magnitude higher  $M^{\text{FC}}$  than the single crystal and bulk [7,8]. The difference between  $M^{\text{FC}}$  and  $M^{\text{ZFC}}$  is plotted with temperature in Fig. 3b. The maximum magnetization value shifts to lower temperature with increase in applied field from  $10$  to  $500$  Oe, which is expected [12–13]. Below  $T_s$ , magnetization again increases. Though  $M^{\text{ZFC}}$  shows a peak for both superparamagnets and spin glasses, the temperature dependence of FC susceptibility becomes saturated below the peak temperature for spin glasses and continues to increase below that temperature for superparamagnets [14]. The increasing tendency of magnetization below  $T_s$  (Fig. 3a) shows therefore an evidence of superparamagnets. The temperature dependence of ac susceptibility measured at several frequencies ranging from  $3$  to  $1000$  Hz probes further the spin glass (SG) and SPM behavior. The sample is first cooled from room temperature to  $10$  K in a

zero magnetic field. Then a probing ac magnetic field of 3.0 Oe is applied to measure the susceptibility as the temperature is slowly raised. Fig. 4a and b shows the real and imaginary parts of susceptibility. We note that  $\chi'$  decreases with increase in frequency, showing that  $\chi'_{\max}$  is independent of frequency, which eliminates the possibility of spin glass behavior. Such frequency independent behavior has also been observed in other nanoparticle system [15].  $\chi'_{\max}$  does not change with temperature and frequency.  $\chi''$  shows a peak at low temperature ( $\sim 23$  K) corresponding to  $T_s$ .  $T_c$  at 97 K and  $T_s$  at 23 K, associated with the transition from paramagnetic to long range ferrimagnetic and from long range ferrimagnetic to long/short range spiral magnetic structures, respectively, are in broad agreement with the specific heat versus temperature measurement (figure not shown here).

The variations in magnetization with applied magnetic field at several temperatures after ZFC are shown in Fig. 5. Above  $T_c$ , the  $M$  versus  $H$  taken at 100 K shown in Fig. 5a confirms the paramagnetic phase. Below  $T_c$ , i.e. at 60 and 80 K, we do not

observe any hysteresis (Fig. 5b). Magnetization readily increases at low field and then linearly increases up to the maximum applied field (60 kOe). At 50 K, we observed hysteresis loop with non-saturation of magnetization up to maximum applied field of 60 kOe (Fig. 5c). While long range ferrimagnetic phase below  $T_c$  has been seen in bulk phase [8], the absence of hysteresis loop at 60 and 80 K eliminates such long range ferrimagnetic order in these nanoparticles below  $T_c$ , which persists up to 60 K. The appearance of loop at 50 K and its disappearance at 60 K suggest that the nanoparticles are SPM in nature and the blocking temperature is between 50 and 60 K. The definition of SPM materials meets at least two requirements. First, above  $T_b$ , the system must not show any hysteresis, which we observed at 60 K. Second, the magnetization curve must be temperature dependent to the extent that curves taken at different temperatures must (approximately) superimpose when being plotted against  $H/T$  [16]. The plot of magnetization versus  $H/T$  measured at 60 and 80 K shown in Fig. 6 confirms the SPM phase below  $T_c$ . In contrast

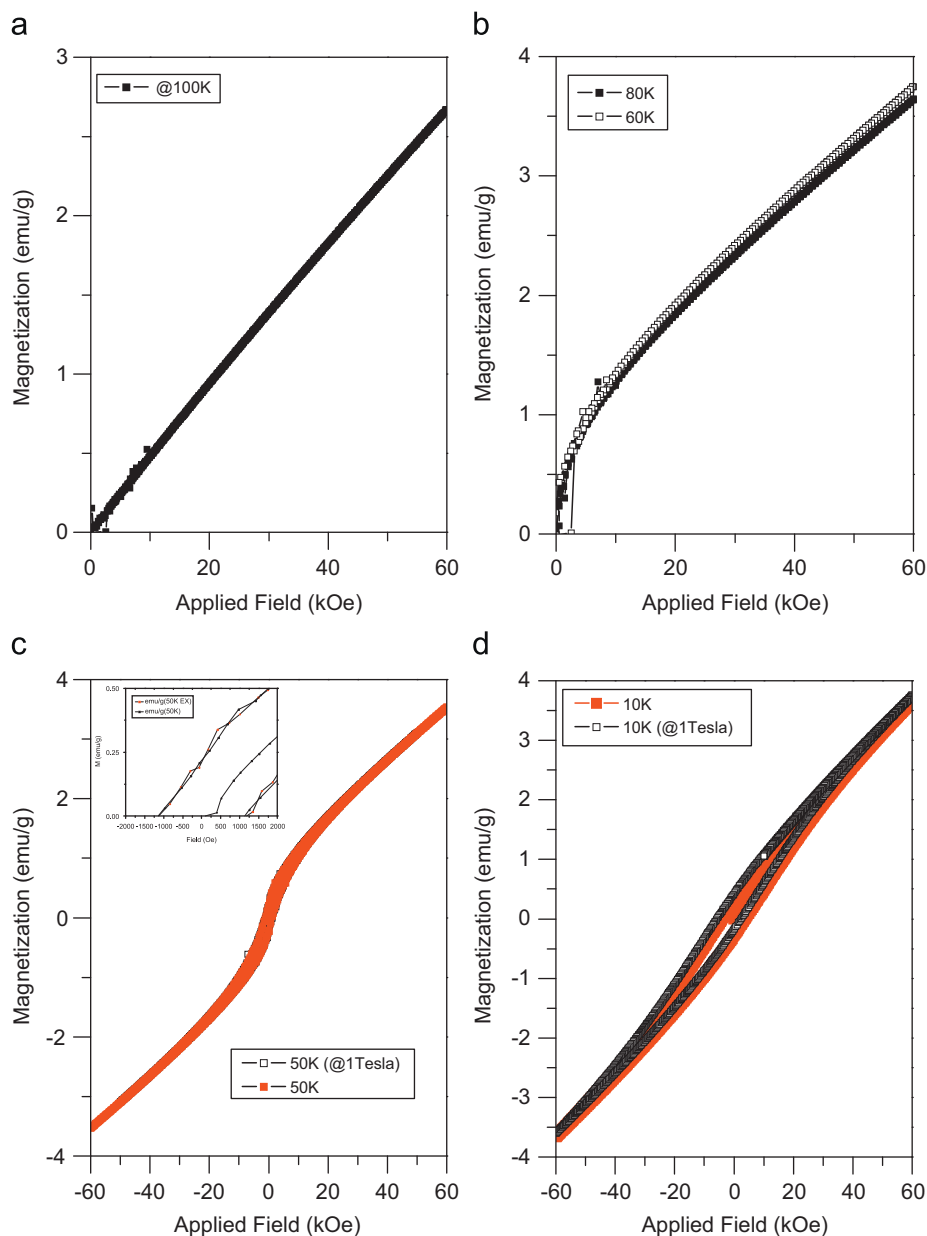


**Fig. 5.** Magnetization versus applied magnetic field measured at (a) 100 K, (b) 80 and 60 K, (c) 50 K and (d) 10 K of CoCr<sub>2</sub>O<sub>4</sub> nanoparticles calcined at 600 °C. In (c) and (d) measurement of magnetization with varying external field after cooling under 10 kOe magnetic field at 50 and 10 K are shown respectively.

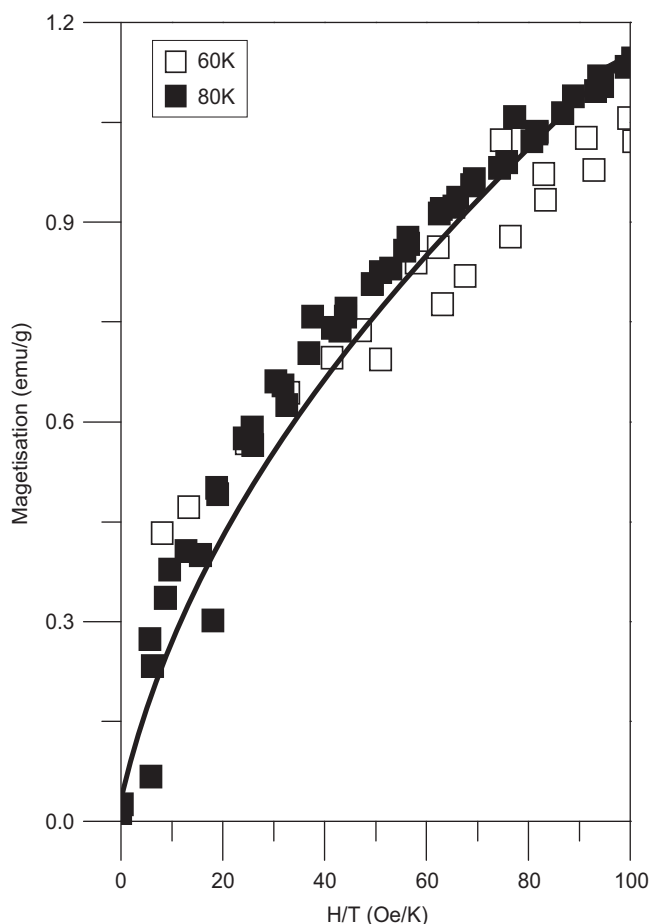


Fig. 6. Magnetization  $M$  as a function of  $H/T$  at  $T=60$  and  $80$  K of  $\text{CoCr}_2\text{O}_4$  nanoparticles calcined at  $600$  °C.

to paramagnetic to ferrimagnetic phase transition at  $T_c$  in bulk  $\text{CoCr}_2\text{O}_4$ , we observed paramagnetic to a SPM phase followed by a long range ferrimagnetic phase. The intermediate SPM phase has not been observed even in nanoparticles of cobalt chromite prepared by sonochemical method [17].

Other interesting feature to be noted here is the exchange bias phenomenon that is generally reported at the ferromagnetic–antiferromagnetic (FM–AFM) interface in thin films, also observed in nanoparticles of  $\text{CoCr}_2\text{O}_4$ . We have carried out the measurement of magnetization with varying external field after cooling under  $10$  kOe magnetic field at  $50$  and  $10$  K (Fig. 5c and d).  $M$  versus  $H$  loop at  $50$  K shows neither a shift in the hysteresis loop nor enhancement in  $H_c$  without shifting of the loop (Fig. 5c and the inset). At  $10$  K, we observed shifting of the loop as well as an enhancement in  $H_c$  by  $250$  Oe than in  $H_c$  measured without cooling under magnetic field (Fig. 5d). In addition, coercivities at  $50$  K ( $\sim 1.1$  kOe) and  $10$  K ( $\sim 4.5$  kOe) show an order of magnitude higher than  $H_c$  reported for single crystals [7].

In fact, the exchange bias phenomenon has been analyzed in terms of an alignment of the AFM spins at FM–AFM interface parallel to FM spins occurring during the field cooling procedure. The coupling between AFM and FM spins at the interface exerts an additional torque on the FM spins, which has to be overcome

by the external field. Depending on the strength of the AFM anisotropy, one may find a shift in hysteresis loop or enhancement in  $H_c$  without any loop shift during field cooling procedure ([18] and references there in). On the other hand, both effects may also be observed simultaneously due to for example structural defects or grain size distribution ([18] and references there in). The origin of  $H_c$  enhancement with shifting of loop observed at  $10$  K could be ascribed to the distribution of particles, which is observed from FESEM and disordered spin configuration existing at the surface evidenced from the non-saturation of magnetization and one order magnitude higher  $H_c$ . The absence of loop shift or absence of  $H_c$  change at  $50$  K further confirms the blocking temperature of SPM phase [18–20].

#### 4. Conclusion

Nanoparticles of cobalt chromite synthesized through conventional coprecipitation technique undergo paramagnetic to superparamagnetic phase transition at  $T_c$  in contrast with paramagnetic to ferrimagnetic phase transition in bulk. Further decrease in temperature transforms superparamagnetic to long range ferrimagnetic phase keeping  $T_c$  and  $T_s$  almost the same as in the bulk phase. The blocking temperature of superparamagnetic phase lies in between  $50$  and  $60$  K. Exchange bias phenomenon has been observed in these nanoparticles of  $\text{CoCr}_2\text{O}_4$ . The absence of loop shift or absence of enhancement in  $H_c$  at  $50$  K supports the blocking temperature of SPM phase.

#### Acknowledgments

UGC-DAE Consortium for Scientific Research (CSR), Indore, is acknowledged for the support. DST, Government of India, is acknowledged for funding the 14T-PPMS-VSM for magnetic measurement at CSR, Indore.

#### References

- [1] Y. Yamasaki, S. Miyasaka, Y. Kaneko, J.-P. He, T. Arima, Y. Tokura, Phys. Rev. Lett. 96 (2006) 207204.
- [2] A. Broese Van Groenou, P.F. Bergers, A.L. Stuyts, Mater. Sci. Eng. 3 (1969) 317.
- [3] Y. Yafet, C. Kittel, Phys. Rev. 87 (1952) 290.
- [4] T.A. Kaplan, K. Dwight, D.H. Lyons, M. Menyuk, J. Appl. Phys. 32 (1961) 13S.
- [5] T.A. Kaplan, Phys. Rev. 116 (1959) 888.
- [6] N. Menyuk, K. Dwight, A.L. Wold, J. Phys. 25 (1964) 528.
- [7] K. Tomiyasu, J. Fukunaga, H. Suzuki, Phys. Rev. B 70 (2004) 214434.
- [8] G. Lawes, B. Melot, K. Page, C. Ederer, M.A. Hayward, Th. Proffen, R. Seshadri, Phys. Rev. B 74 (2006) 024413.
- [9] Y.J. Choi, J. Okamoto, D.J. Huang, K.S. Chao, H.J. Lin, C.T. Chen, M. van Veenendaal, T.A. Kaplan, S.W. Cheong, Phys. Rev. Lett. 102 (2009) 067601.
- [10] C. Rath, K.K. Sahu, S. Anand, S.K. Date, N.C. Mishra, R.P. Das, J. Magn. Mater. 202 (1999) 77.
- [11] C. Rath, S. Anand, R.P. Das, K.K. Sahu, S.D. Kulkarni, S.K. Date, N.C. Mishra, J. Appl. Phys. 91 (2002) 4.
- [12] S.D. Tiwari, K.P. Rajeev, Phys. Rev. B 72 (2005) 104433.
- [13] M. Hanson, C. Johansson, S. Morup, J. Phys.: Condens. Matter 7 (1995) 9263.
- [14] T. Bitoh, K. Ohba, M. Takamatsu, T. Shirane, S. Chikazawa, J. Phys. Soc. Jpn. 64 (1995) 1305.
- [15] T. Jonsson, P. Nordblad, P. Svedlindh, Phys. Rev. B 57 (1998) 497.
- [16] C.P. Bean, I.S. Jacobs, J. Appl. Phys. 27 (1956) 1448.
- [17] D.P. Dutta, J. Manjanna, A.K. Tyagi, J. Appl. Phys. 106 (2009) 043915.
- [18] J. Nogues, J. Sort, V. Langlais, V. Skumryev, J.S. Munoz Surinaeb, M.D. Baro, Phys. Rep. 422 (2005) 65.
- [19] S.M. Zhou, K. Liu, C.L. Chien, J. Appl. Phys. 87 (2000) 6659.
- [20] A.J. Devasahayam, M.H. Kryder, J. Appl. Phys. 85 (1999) 5519.